Research Square

Preprints are preliminary reports that have not undergone peer review.
They should not be considered conclusive, used to inform clinical practice,
or referenced by the media as validated information.

Plant Extract Composition Driven Optimization of Green-Synthesized ZnO Nanoparticles for Enhanced Seedling Growth

Shuchi Verma
shuchiverma@ramjas.du.ac.in
University of Delhi
Anushka Garg
University of Delhi
Shifa Ahmed
University of Delhi
Navneet Nayan
University of Delhi
Serene shimar
University of Delhi
Siya Roopdaska
University of Delhi
Aryan Mishra
University of Delhi
Pushpanjali Singh
University of Delhi

Research Article

Keywords: seed priming, extract biochemical composition, nanoparticle functional performance optimization

Posted Date: November 17th, 2026

DOI: https://doi.org/10.21203/rs.3.rs-11740434/v1

License: This work is licensed under a Creative Commons Attribution 4.0 International License.
Read Full License

Additional Declarations: No competing interests reported.

Plant Extract Composition Driven Optimization of Green-Synthesized ZnO Nanoparticles for Enhanced Seedling Growth

Shuchi Verma, * Anushka Garg[1], Shifa Ahmed[1], Navneet Nayan[1], Serene Shimar [1], Siya Roopdaska[1], Aryan Mishra,[1] Pushpanjali Singh[1]

[1]Department of Chemistry, Ramjas College, University of Delhi, 110007, New Delhi, India.

[2] Gaudhan Research Laboratory, Ramjas College, University of Delhi,110007, New Delhi, India.

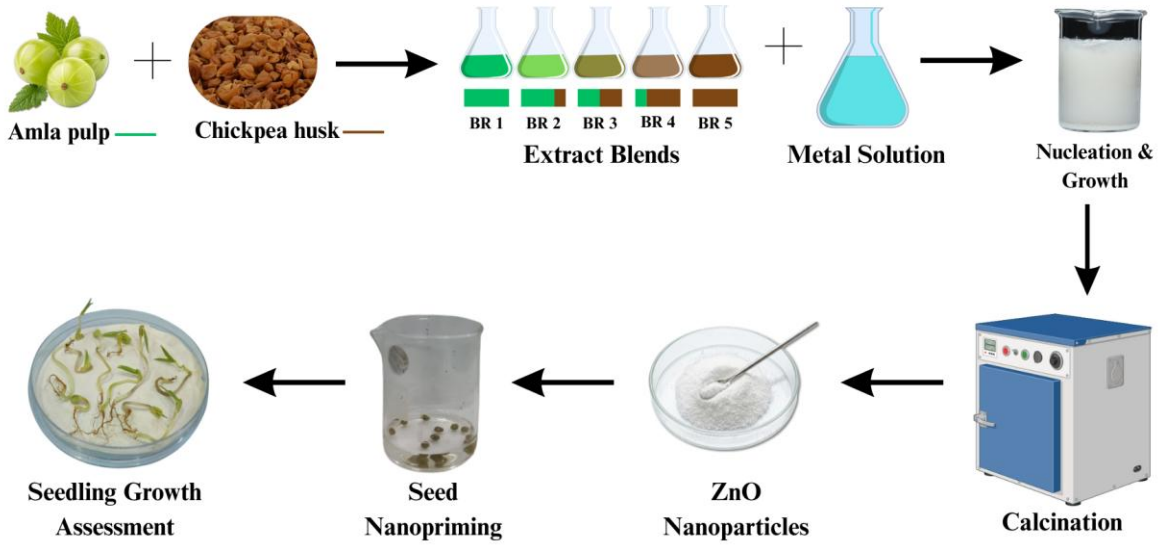
***Correspondence author: Email id- shuchiverma@ramjas.du.ac.in**

Orcid Id - 0009-0000-8064-740X

ABSTRACT

Green synthesis of zinc oxide nanoparticles (ZnO NPs) using plant extracts offers an eco-friendly route to nano-agricultural inputs. However, the relative effect of extract composition and nanoparticle size on seed priming performance remains unclear, as these factors are usually studied independently. ZnO NPs were synthesized from different amla:chickpea husk extract ratios (100:0, 75:25, 50:50, 25:75, and 0:100) and applied under fixed exposure conditions to explore how extract composition and particle size are associated with seed germination and seedling growth. Extracts were evaluated for DPPH radical-scavenging activity, protein, and carbohydrate content, while the nanoparticles were characterized by UV-Vis, FTIR, XRD, and SEM. Primed *Vigna radiata* seeds (65.5 µg mL^{-1}, 6 h) were evaluated after seven days for germination, growth, and vigor index. All formulations yielded crystalline hexagonal wurtzite ZnO NPs. The 50:50 formulation had the highest DPPH activity (84.92%) and the largest shoot length (4.40 cm), root length (2.59 cm), and vigor index (6.99). Across the five formulations, DPPH activity showed a strong positive correlation with shoot length ($r = 0.892$, $p = 0.042$) and root length ($r = 0.889$, $p = 0.044$). Protein content showed a strong negative correlation with nanoparticle diameter ($r = -0.879$, $p = 0.0495$), suggesting extract composition was related to particle size, although this did not translate into growth effects. These findings suggest that, under fixed exposure conditions, extract composition was more closely associated with seed-priming performance than particle size, identifying blend composition as a tunable and underexplored variable in green ZnO NP synthesis.

Keywords: seed priming; extract biochemical composition; nanoparticle functional performance optimization.



Introduction

Nanotechnology has revolutionized agricultural technology, and engineered nanomaterials are being developed as a new category of agricultural inputs to overcome the limitations and ecological effects of conventional fertilization and crop protection [1,2]. Nanofertilizers and nanopesticides supply nutrients and active ingredients in a controlled manner, increasing plant uptake while reducing losses from leaching, volatilization, and degradation [3]. Their high surface-area-to-volume ratios and adjustable surface chemistry enhance solubility, bioavailability, and delivery accuracy, making nanotechnology a crucial component of precision-based and sustainable agriculture [4].

However, the way these nanomaterials are produced remains a concern. Traditional physical and chemical routes, such as polyol reduction, thermal decomposition, and vapour deposition, often require high temperature, high pressure, specialized equipment, and hazardous reducing agents like sodium borohydride and hydrazine hydrate [5,6,7]. Although these techniques allow shape-controlled synthesis, they generate toxic residues and hazardous by-products and demand significant energy and cost, making them unsuitable for agriculture, where nanoparticles are intentionally introduced into soil and plant systems [8,9,10]. Plant-mediated green synthesis has therefore gained attention as an environmentally friendly, cost-effective alternative that operates at ambient temperature and pressure, without toxic solvents, using plant extracts in place of synthetic reducing and capping agents [8,10,11]. Comparative studies show that green-synthesized metal nanoparticles are smaller, more uniform, and less toxic in biological test systems than chemically synthesized counterparts of the same metal, while retaining their useful functional properties [10].

A key reason green synthesis works is that plant extracts do not merely replace a single synthetic compound; they perform two roles that conventional chemistry achieves with separate reagents. Reducing phytochemicals such as polyphenols, flavonoids, and ascorbic acid donate electrons to metal ions and initiate nucleation [5,12], whereas proteins, carbohydrates, and other phytochemicals adhere to the surfaces of emerging nuclei and act as capping and stabilizing agents that halt growth and regulate final size, shape, agglomeration, and dispersity [11,13,14]. Chemical synthesis, in contrast, generally pairs a toxic reducing agent with a separate synthetic capping agent such as polyvinylpyrrolidone [15,16]. This intrinsic chemical complexity stems from the presence of several molecules within the extract that simultaneously act as reducing and stabilizing agents, making it central to a successful synthesis [17], because the extract's phytochemical composition fulfils both roles, the properties of the resulting nanoparticles depend directly on the plant source [8,11]. The relative reducing and stabilizing activity affects the balance between nucleation and growth [9,13], and thereby particle size and dispersity; accordingly, low reductant concentrations yield larger, more asymmetrical particles, whereas high concentrations cause explosive nucleation [18].

Metal oxides form an important class of these nanomaterials, and among them, zinc oxide nanoparticles (ZnO NPs) are particularly relevant because zinc is an essential micronutrient that serves as a structural and catalytic cofactor in many enzymes, is necessary for auxin production, supports chlorophyll formation, and helps maintain membrane integrity [19,20,21]. Zinc deficiency is among the most prevalent micronutrient deficiencies in agricultural soils and adversely affects crop productivity globally [20]. The efficient uptake of ZnO NPs, combined with their high surface reactivity and solubility, places them where micronutrient delivery meets nanotechnology [22,23], and several studies report that they enhance seed germination,

seedling vigour, and plant growth and increase protein and chlorophyll concentrations, supporting their use as nanofertilizers [24,25].

The reducer–stabilizer balance matters beyond particle dimensions, because it also shapes how ZnO NPs behave once they contact a plant system. Particle size and surface chemistry are most frequently found to control nanoparticle–plant interactions, affecting both the pathway of entry into plant tissue and the rate at which bioactive ions are released [26]. ZnO NPs dissolve readily in aqueous environments, and smaller particles generally dissolve faster, releasing more Zn^{2+} [27,28]. Root uptake appears to be governed primarily by dissolved zinc concentration, but because dissolution depends on size, size effectively regulates zinc absorption [29], ZnO NPs can thus act as slow-release zinc sources whose solubility can be tuned to balance nutrient supply against phytotoxicity [30]. Surface chemistry also has a significant influence: Zn^{2+} dissolution depends on pH and surface coating [31], and coatings govern suspension stability, transport within plants, and interactions with plant cells [32]. In biogenic synthesis, the biological corona, the phytochemical layer remaining on the particle surface, is not entirely inert but contributes substantially to bioactivity and uptake[33,34, 35]. Differences in surface chemistry and Zn^{2+} release kinetics arising from different extracts are therefore expected to translate into differences in how nanoparticles interact with germinating seeds and developing seedlings.

Despite this expected mechanistic link, the literature shows a fairly uniform trend that leaves an important gap. In most green-synthesis studies, including those on ZnO NPs, a single plant extract serves as the only source of reducing and capping agents; the resulting nanoparticles are characterized (size, shape, band gap), and one or more downstream bioactivity outcomes (antimicrobial, antioxidant, or occasionally plant growth) are reported, generally as a validation step rather than as a deliberately varied factor in the experimental design [14]. Where multiple extracts are used, it is typically to tailor the synthesis itself, improving yield, size uniformity, or stability, rather than to treat the reducer-to-stabilizer ratio as an independent variable tracked through to a functional biological endpoint. Similarly, seed-priming outcomes are usually attributed to dose and particle size, even though evidence suggests that zinc ion release and surface chemistry, rather than particle size per se, govern germination [36].

To address this gap, the present study investigated whether the intentional control of extract composition can be used to adjust ZnO nanoparticles characteristics and the resulting biological effects. ZnO NPs were synthesized across a compositional gradient combining amla, widely reported as a reducer-dominant extract rich in ascorbic acid and polyphenols [37], with chickpea husk, an agricultural residue expected to contribute stabilizing, capping-associated biomolecules such as structural polysaccharides and proteins [38]. By systematically varying the relative reducer-to-stabilizer activity, this binary-blend design allows nucleation-versus-growth kinetics, and consequently the physicochemical characteristics of the nanoparticles, to be investigated. To our knowledge, the novelty of this work lies in linking controlled variation of extract composition to a functional biological endpoint within a single framework. The aim of this study was therefore to characterize the resulting ZnO NPs and evaluate their effects on seed germination and seedling growth, in order to relate blend composition to nanoparticle properties and plant responses, and to identify the blend ratio offering the best combination of nanoparticle properties and functional performance.

Materials and Methods

Synthesis of Plant Extracts

Fresh amla (Phyllanthus emblica) fruit and chickpea (Cicer arietinum) husk were acquired from a local market. To remove the surface debris, both samples were washed thoroughly, followed by a 20 min soak in distilled water. Subsequently, the amla fruit was divided into pieces and ground. For chickpea husk, we followed a process of separation, cleaning, and air-drying before milling it into fine powder in a laboratory ball mill. All chemicals and reagents used were of analytical grade and purchased from Arun Chemicals Pvt. Ltd. (India). Amla and chickpea husk extracts were prepared using solid-to-solvent ratios of 1:4 (w/v) and 1:8 (w/v), respectively. These ratios were selected to obtain workable aqueous extracts for the subsequent green synthesis. The prepared extracts were subjected to a 30 min sonication at room temperature. Individual extracts were then combined to form five blend ratios of amla-to-chickpea-husk extract (v/v), 100:0, 75:25, 50:50, 25:75, and 0:100, hereafter referred to as BR 1, BR 2, BR 3, BR 4, and BR 5, respectively. The blend ratio represented extract composition, and the total extract volume was kept constant across all treatments so that only the amla:husk proportion differed between formulations.

Synthesis of ZnO Nanoparticles

Dropwise additions of each extract combination in various blend ratios were made to a 0.1 M zinc acetate solution (1:1 v/v), and the pH was brought to 9, under constant stiring at room temperature. The mixture was then ultrasonicated for 30 min at 40 °C, during which its color changed from pale yellow to white, and a white precipitate was formed. The precipitate was then allowed to settle, centrifuged three times (5,000 rpm for 10 min each), followed by an ethanol rinse and oven drying. Lastly, the dried powder was calcined in a muffle furnace at 450 °C for 2 h to obtain the final ZnO nanoparticles.

Seed Germination and Seedling Growth Analysis

Seeds of Vigna radiata were used for nano-priming and germination assays, following [42], who determined that the best germination and vigor indices occurred at a concentration of 65.5 µg/mL. The seeds were surface-sterilized through successive washings with distilled water followed by 70% ethanol before being subjected to priming. They were then treated with the prepared ZnO nanoparticle suspension at a rate of 65.5 µg/mL for 6 hours. The nanoparticle concentration was thus fixed across all treatments (BR 1–BR 5), and a distilled water (DW) control was included. After priming, seeds were placed on moistened absorbent paper in Petri dishes and kept at a steady room temperature of 25 °C for a week, following which the lengths of the roots and shoots were measured and the number of germinated seeds was counted. The germination percentage (GP) was calculated using the following formula:

Germination percentage (%) = (Number of germinated seeds / Total number of seeds sown) × 100

The vigor index was determined by multiplying the germination percentage by the mean combined length of shoot and root per seedling, as described by [43]:

SVI = (GP / 100) × (MSL + MRL)

where SVI is the seedling vigor index (cm), GP is the germination percentage (%), MSL is the mean shoot length (cm), and MRL is the mean root length (cm).

.

Characterization of Plant Extracts and Zinc Oxide (ZnO) Nanoparticles

The biochemical composition of each extract blend was characterized before synthesis to investigate whether extract chemistry is associated with the properties and seedling-growth performance of the resulting nanoparticles.

DPPH Radical Scavenging Activity

The DPPH (2,2-diphenyl-1-picrylhydrazyl) radical scavenging assay was used to determine the antioxidant (reducing) capacity of the extracts. Extraction and reaction parameters followed a modified ultrasound-assisted extraction protocol [39] . The process involved mixing 0.2 mL of each sample with 2 mL of 6×10^{-5} M DPPH ethanolic solution. After allowing the reaction to proceed in the dark for 15 min, the corresponding drop in absorbance was measured at 517 nm using a Shimadzu UV-1900i spectrophotometer.

Total Carbohydrate Estimation

Total carbohydrate content was determined using a previously reported phenol-sulfuric acid method [40] . Serial dilutions of the standard (0.2-1.0 mL) and 0.2 mL of the test sample were separately diluted to a final volume of 1 mL with distilled water. In parallel, a reagent blank was prepared under identical conditions. Addition of 1 mL phenol was followed by addition of 5 mL of 96% H_2SO_4 to each sample. The mixtures were allowed to stand undisturbed for 10 min and subsequently incubated in a water bath at 25- 30 °C for 20 min. Glucose was converted into hydroxymethylfurfural by acid-catalyzed dehydration, which produced a green chromophore through its reaction with phenol. The absorbance of this green chromophore was measured at 490 nm using a Shimadzu UV-1900i spectrophotometer. A standard curve was then used to determine the total carbohydrate content.

Protein Estimation

Protein was quantified using trichloroacetic acid (TCA) precipitation and the bicinchoninic acid (BCA) assay [41] which was modified for aqueous plant extracts. To reach a final TCA concentration of roughly 10% (w/v), which was selected to improve precipitation efficiency over a wide range of protein concentrations in contrast to the original protocol, 100 µL of 6.1 N TCA stock was added dropwise along the tube wall in 900 µL of extract. After the samples were vortexed for 30 seconds and then incubated on ice for 30 minutes (a duration extended from the original 15 minutes to maximize pellet formation in dilute plant extracts), which was then centrifuged for 15 minutes at 4°C and 14,000 rpm. The pellet that remains after the elimination of the supernatant that contained pigments, polyphenols, and other non-protein interferents were resuspended in 900 µL of resuspension buffer (10 mM Tris, pH 7.5, and 10 mM sodium bicarbonate, 1:1 v/v), vortexed for 15-20 minutes, and the protein content was subsequently measured by the BCA assay using a standard curve of bovine serum albumin prepared in the same buffer matrix.

Characterization Techniques

The synthesized ZnO nanoparticles were characterized using X-ray diffraction (XRD; PANalytical Aeris tabletop X-ray diffractometer, Cu-Kα radiation, λ = 1.5418 Å, 2θ range of 5–90°) to determine their crystalline structure; Fourier-transform infrared (FTIR) spectroscopy (Nicolet iS50 FTIR spectrometer equipped with a tri-detector DLaTGS detector with a KBr window) to identify surface functional groups; and field-emission scanning electron microscopy (FESEM; Gemini SEM 500) to investigate surface morphology and particle size. The FESEM analysis was performed using an accelerating voltage range of 0.02–30 kV, a magnification range of 50×–2,000,000×, a probe current of 3 pA–20 μA (up to 100 nA optional), and a working distance of 0.1mm–50m. The Shimadzu UV-1900i UV-Vis spectrophotometer was used to measure UV-Vis absorption spectra of synthesized nanoparticle in range of 200-600nm.

Statistical Analysis

Replicate seeds within each treatment were used to measure seedling growth and germination; the results are shown as mean values. Two composite indices were computed using this data: the germination percentage, which is defined as the percentage of seeds in a group that produced radicle and/or shoot emergence and the vigor index, which is determined by multiplying the germination percentage by the mean combined length of shoot and root per seedling, as described by [43]. Analysis was carried out to evaluate the relationship between two growth parameters (mean shoot length and mean root length) and extract/nanoparticle characteristics (DPPH radical-scavenging activity, carbohydrate content, protein content, and mean particle diameter); Pearson correlation coefficients were generated using the mean values at each of the five blend levels. The significance level was set at $\alpha = 0.05$, two-tailed p-values ($df = n-2 = 3$) and 95% confidence intervals are reported. All statistical analyses were carried out using jamovi (version 2.5, The jamovi project, 2024).

Results and Discussion

Extract characterization across blend ratios

The biochemical and physicochemical profiles of the different blends in the synthesis series varied significantly, as presented in Table 1. In the case of DPPH radical scavenging, the trend was non-linear, with maximum activity at the blend ratio of 50:50 and a decline toward both compositional extremes. Carbohydrate content decreased steadily with an increase in the proportion of chickpea husk, whereas protein content showed no consistent directional trend.

The measured particle diameter varied between 36.55 and 62.67 nm and did not show a progressive change across the different blend compositions. Amla-dominant treatment resulted in the smallest particle size, whereas the largest particle size was observed in the husk-dominant treatment and 75:25 blend. This non-linear pattern indicates that particle formation was influenced by the combined biochemical environment of the extracts rather than by the proportion of either extract alone.

A few tightly coupled processes are involved in forming nanoparticles through plant-mediated methods, including reduction, nucleation, stabilization, aggregation, and capping. Variation in the makeup of the plant extract may therefore produce non-linear changes in the characteristics of the resulting nanoparticles since the same phytochemical can participate in more than one process [8,13].

Table 1. Biochemical and physicochemical characterization of amla:chickpea-husk extract blends

Sample	Blend (Amla: Husk)	DPPH inhibition (%)	Carbohydrate (mg/mL)	Protein (mg/mL)	Particle diameter (nm)
BR 1	100:0	74.26	420.69	0.0443	36.55
BR 2	75:25	82.46	330.19	0.0101	58.25
BR 3	50:50	84.92	256.01	0.0392	44.68
BR 4	25:75	71.48	202.97	0.0599	41.67
BR 5	0:100	68.03	82.57	0.0156	62.67

Physicochemical Characterization and Surface Functionalization of ZnO Nanoparticles

For the synthesis of nanoparticles, the five blend treatments were characterized using UV–visible spectroscopy, FTIR, XRD, and SEM discussed below:

UV–Visible Spectroscopy

The UV-Vis absorption spectra of all five of the samples made from the blends in Fig.1(a) showed that the formation of ZnO nanoparticles occurred throughout the entire range of the blend series and verified by the presence of absorption bands between 300 and 400 nm, which is typical for the transition from the valence to conduction bands of ZnO. In the region of 368.5–371.5 nm – three samples (BR 3, BR 4, BR 5) exhibited well-resolved absorption maxima, whereas BR 1 and BR 2 showed comparatively broadened or flattened absorption features; since peak shape in this region can be influenced by particle size distribution, surface defects, and residual extract-derived organic matter, it is not taken here as a direct measure of particle uniformity.

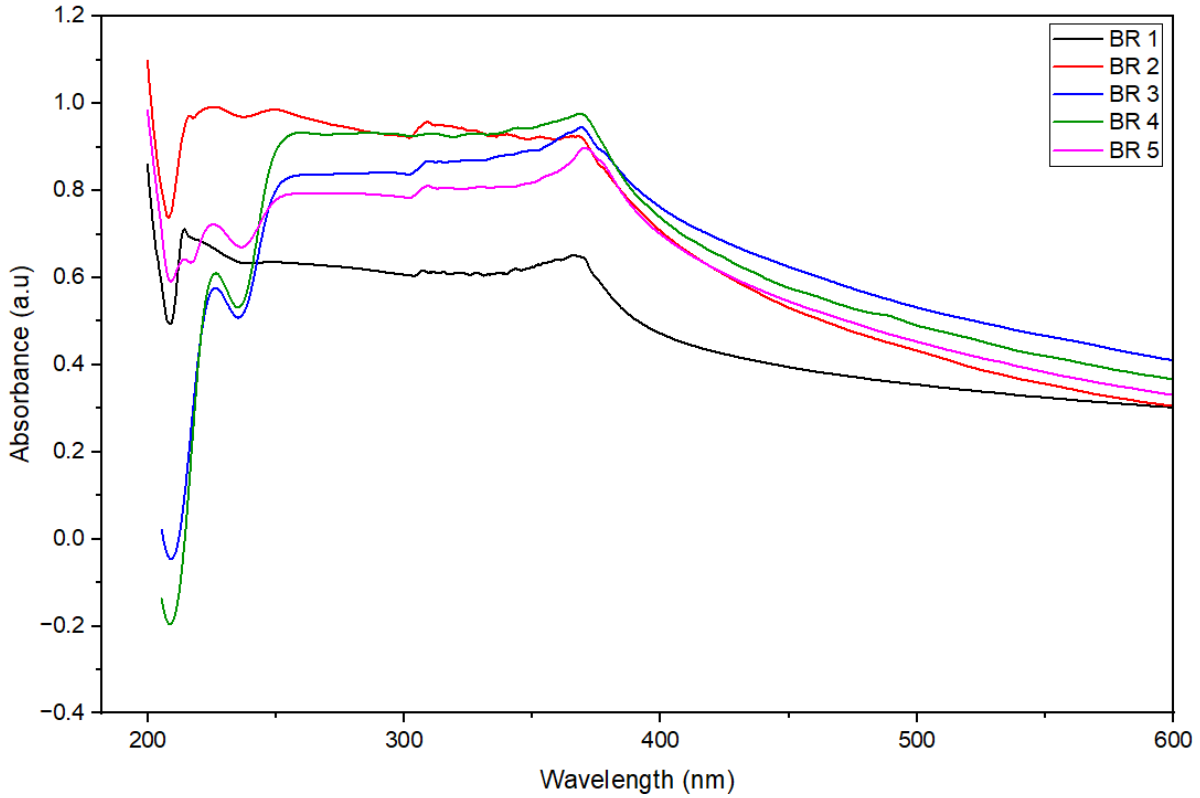


Fig. 1(a): UV-Vis absorption spectra of synthesized ZnO nanoparticle samples BR 1 to BR 5 recorded over the 200–600 nm range.

The optical band gaps were determined by the Tauc method shown in Fig. 1b, and were found to be very close to each other in all 5 blends, ranging from 2.83 eV to 2.93 eV, which is lower than the commonly reported band gap of the bulk ZnO (3.37 eV) [44]. This reduction is not expected to arise from quantum confinement at these particle sizes and is more commonly attributed to defect states (such as oxygen vacancies and zinc interstitials), surface states, and residual extract -derived organic species that add sub-band-gap absorption, all of which may contribute here. The narrow spread of values suggests that blend composition had little effect on the electronic structure. It should also be noted that band gaps of 2.83-2.93 eV are lower than the 3.35 eV that corresponds to the absorption maxima near 370 nm, which may reflect a visible-region absorption tail influencing the linear extrapolation of the Tauc plots.

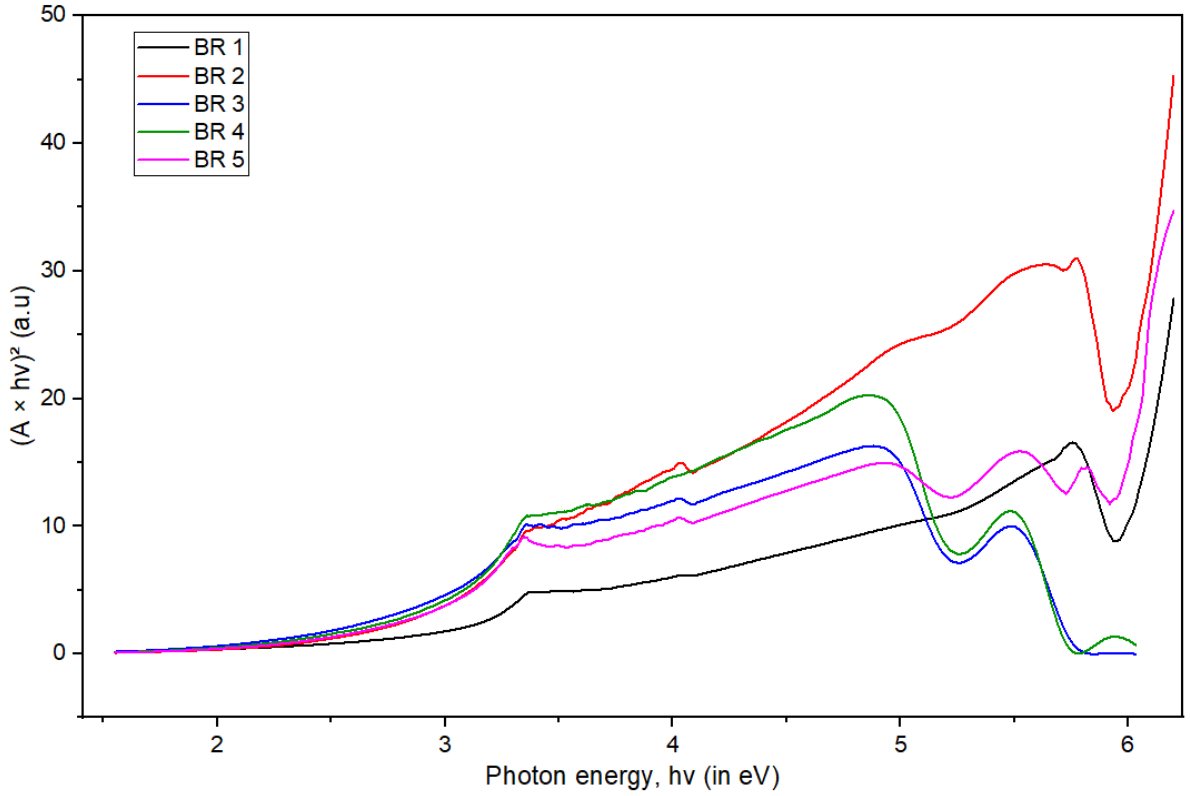


Fig.1(b): Tauc plots [(Ahν)² vs. photon energy] of BR 1 to BR 5 used to estimate the optical band gap of each sample by linear extrapolation of the absorption edge to the x-axis.

FTIR Spectroscopy

The functional groups associated with the synthesized ZnO nanoparticles and the contribution of biomolecules from the extracts to nanoparticle formation and surface stabilization were analyzed using Fourier-transform infrared (FTIR) spectroscopy. Fig. 2 shows the FTIR spectra of the five samples (BR1–BR5). The spectra showed bands corresponding to oxygen-containing organic groups, along with a characteristic low-wavenumber band associated with Zn–O vibrations. The position and relative intensity of these bands differed among the samples and may be related to differences in the chemical composition of the amla and chickpea-husk extracts used for nanoparticle synthesis.

For each band, the reported range reflects the spread of peak positions observed across the five samples (BR1–BR5). The most prominent low-wavenumber feature was the band at approximately 420-457 cm^{-1}. The absorption bands lies within the characteristic 400–600 cm^{-1} region which is specifically assigned to Zn–O stretching vibrations [45]. Therefore, providing strong FTIR evidence for the formation of ZnO nanoparticles.

A broad band was observed at 3350-3450 cm^{-1}. This region falls within the 3200-3600 cm^{-1} range reported to be associated with hydrogen-bonded groups in plant-mediated ZnO systems [46]. The spectra showed a band at approximately 1500-1520 cm^{-1}. The comparative study reported vibrations associated with C=C and C=O functional groups in plant extracts and synthesized ZnO samples, and this band falls within the 1500–1780 cm^{-1} region [47]. This band may therefore be related to the presence of extract-derived organic constituents containing

these functional groups that remained associated with the synthesized nanoparticles. Another band was observed at approximately 1377-1420 cm^{-1}. This band falls within the 1370–1450 cm^{-1} range reported for C–O stretching and/or C–C–C vibrational modes in the plant-mediated ZnO system [47]. Also an additional band was observed at approximately 858-875 cm^{-1}. This band lies within the 738–880 cm^{-1} range reported for Zn–OH-related vibrations in synthesized ZnO samples [47]. The presence of bands associated with oxygen-containing organic groups, along with the characteristic Zn–O vibration, suggests the presence of both the ZnO inorganic phase and extract-derived organic species associated with the nanoparticle surface. This is in line with the proposed role of plant-derived phytochemicals during green synthesis, where hydroxyl and other oxygen-containing compounds can interact with zinc species and may subsequently remain associated with the surface of the formed nanoparticles [48].

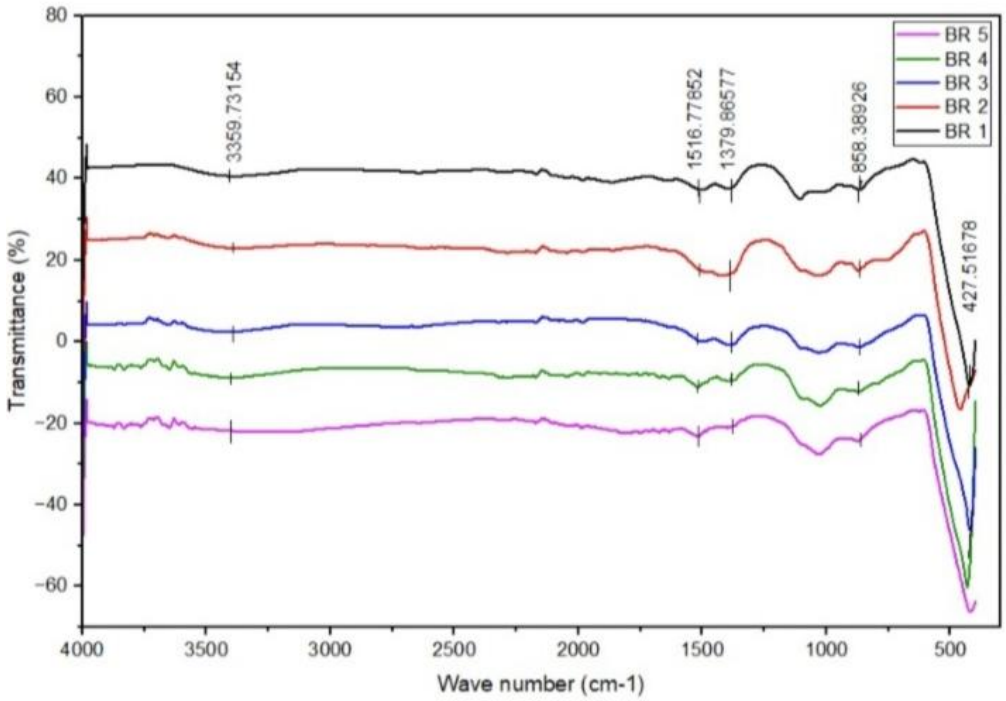


Fig. 2 FTIR spectra of ZnO nanoparticles synthesized using amla and chickpea-husk extracts at five blend ratios (BR1–BR5).

XRD Analysis

The ZnO nanoparticles obtained from the five different blend ratios (BR 1-BR 5) were analyzed by XRD to identify the crystalline phase formed and estimate the crystallite size of each sample. The XRD patterns were anticipated to reflect the formation of ZnO with characteristic peaks of the hexagonal wurtzite phase, as evidenced by the UV-Vis and FTIR analyses in the blend series and to enable the extraction of a crystallite size for each blend for comparison with the particle sizes measured by SEM.

The X-ray diffraction (XRD) patterns of the samples BR 1–BR 5 are presented in Fig. 3. The diffraction peaks of all the samples were very sharp indicating the crystallinity of the

synthesized material. The most prominent reflections from the samples were assigned to the hexagonal wurtzite structure of ZnO [49] per the standard diffraction pattern (JCPDS Card No. 36-1451) and are in accordance with the standard diffraction pattern. Eight common reflections, corresponding to the (100), (002), (101), (102), (110), (103), (112), and (201) planes, were observed across all five samples [50,51] indicating that the major crystalline phase was the same for all five blend treatments, irrespective of blend ratio. The principal diffraction peaks were observed in the approximate 2θ ranges of 31.94–32.24°, 34.60–34.92°, 36.45–36.69°, 47.73–47.95°, 56.71–57.08°, 62.94–63.20°, 68.04–68.34°, and 69.20–69.46° for the (100), (002), (101), (102), (110), (103), (112), and (201) reflections, respectively. Small differences in the position of peaks and the broadening of the peaks were observed among the samples, which may reflect the variations in crystallographic strain and crystallite size of the different blends.

The full width at half maximum (FWHM) of the diffraction peaks was used to approximate the crystallite size using the Debye-Scherrer equation [52]:

$$D = k\lambda / (\beta \cos \theta)$$

where D is the crystallite size, k is the Scherrer constant (0.94), λ is the X-ray wavelength (1.5418Å for Cu-Kα radiation) and β is the FWHM in radians and θ is the Bragg diffraction angle. For comparison, 8 common, well-resolved reflections were chosen for the calculation of the mean crystallite size of the five samples studied. The calculated average crystallite sizes were 26.10 ± 6.43 nm, 29.04 ± 7.67 nm, 29.97 ± 6.90 nm, 22.65 ± 4.80 nm, and 33.57 ± 8.35 nm for BR 1, BR 2, BR 3, BR 4, and BR 5, respectively. The mean crystallite sizes of the blend series were small with BR 5 exhibiting the highest mean size and BR 4 the lowest, which is about 1.5 times the difference. The crystallite sizes are in the range typically reported for biomass/green-synthesized ZnO nanoparticles [53] and indicates that the synthesis method employed in the present work is generally in line with previous work in the literature with a crystallite size dependent on the blend used and measurable.

Combined with the particle size distribution measured by SEM, the crystallite size derived here would be expected to be smaller than the corresponding particle diameter determined by SEM for all the samples because XRD crystallite size represents the size of each single coherently-diffracting crystalline domain while SEM particle diameter represents the size of any agglomeration of multiple such domains into a single particle observed. Notably, BR 5 with the largest crystallite size (33.57 nm) had comparatively large SEM particle size (62.7 nm) compared to sample BR 4 with the smallest crystallite size (22.65 nm), which had large SEM particle size (41.7 nm). This suggests that, in the case of BR 5 in particular, the observed large particle size in SEM is much more likely to be due to aggregations of crystallites after the nucleation than to the crystallite size difference between BR 4 and BR 5 (22.65 vs. 33.57 nm), assuming that the former is proportionally larger in crystallite size. This pattern may also be related to the biomolecule composition of the blends (Table 1): BR 5, having the lowest carbohydrate content, may offer comparatively weaker capping, allowing more crystal growth, whereas BR 4, despite its low carbohydrate content, has the highest protein content and the smallest crystallite size, suggesting that proteins may act as a more efficient capping agent restricting crystal formation.

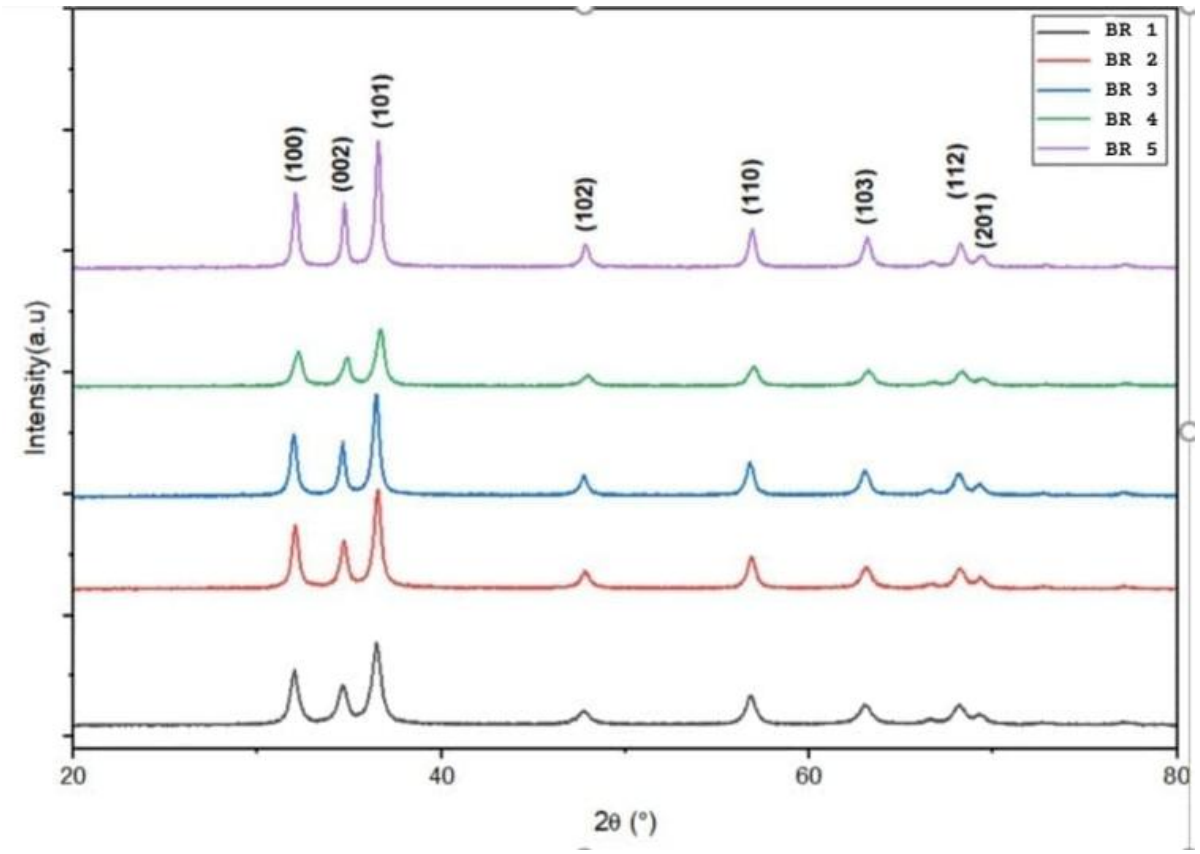


Fig. 3 XRD patterns of ZnO nanoparticles (BR 1 to BR 5).

SEM Analysis and Particle Size Distribution

The ZnO nanoparticles for blends of each ratio were analysed by SEM imaging using ImageJ software to gain a direct examination of the morphology and quantify the particle size distribution for each sample. The SEM results were anticipated to show differences in particle shape and size within the blend series as XRD had already confirmed all five blends to be in the same crystalline phase without describing the particle shape and size, and thereby allow comparison with the crystallite size calculated from the XRD data.

The SEM image shown in Fig. 4(a-e) revealed that the particle morphology differed significantly from one blend in the blend series to another. BR 1 and BR 2 had relatively fine, close clusters while BR 3 had a combination of fused sheet-like areas and rounded particles; BR 4 had coarser angular clusters, and BR 5 had larger, denser agglomerates that were easily distinguished from the other four. Particle size analysis quantified this trend: mean diameters were 36.6 ± 9.6 nm (BR 1), 58.3 ± 16.0 nm (BR 2), 44.7 ± 13.6 nm (BR 3), 41.7 ± 17.1 nm (BR 4), and 62.7 ± 19.1 nm (BR 5). All five blends fall within a broadly similar 35-65 nm size range, with BR 5 giving the largest mean diameter and BR 1 the smallest – roughly 1.7-fold difference across the series- indicating that the blend ratio used in BR 5 allowed for somewhat more particle growth or aggregation than the other blends, while BR 2 and BR 3 occupy an intermediate range. This trend may possibly be attributed to the carbohydrate content of the blends (Table 1), which is lowest in BR 5 and highest in BR 1; a lower carbohydrate content could imply comparatively weaker capping/stabilizing action, allowing greater particle growth in BR 5, whereas the higher carbohydrate content in BR 1 may be indicative of more efficient

capping that restricts particle growth. However, since BR 2 has the second highest carbohydrate content but a comparatively large particle size, protein content (lowest in BR 2 and BR 5, the two blends with the largest particle size) may also contribute to capping, so the observed sizes may reflect the combined effect of both biomolecule classes.

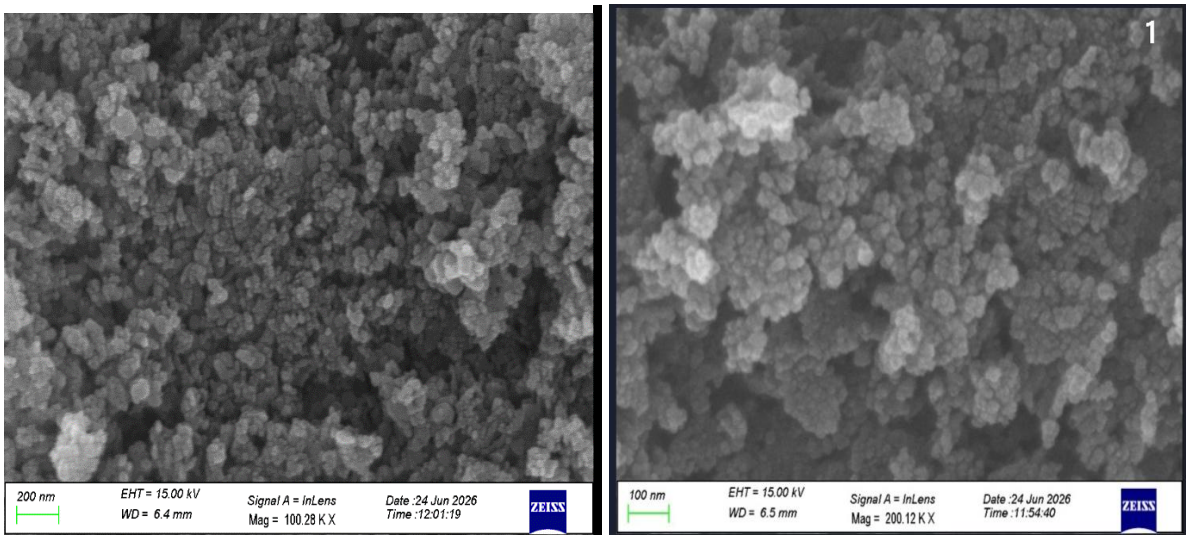


Fig. 4(a): Morphology of sample BR 1 at two different magnifications.

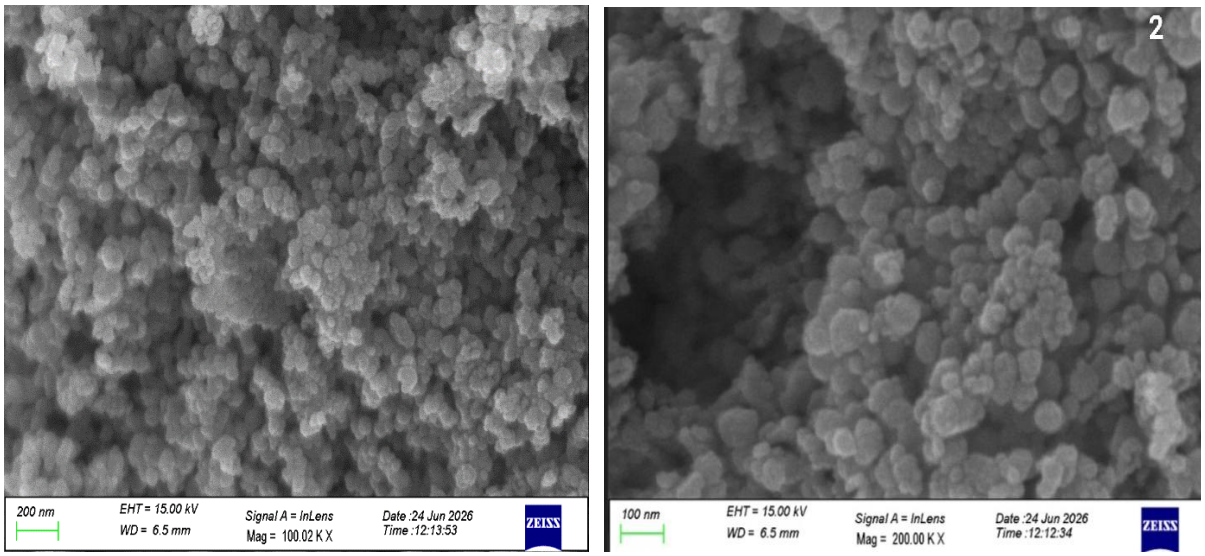


Fig. 4(b): Morphology of sample BR 2 at two different magnifications.

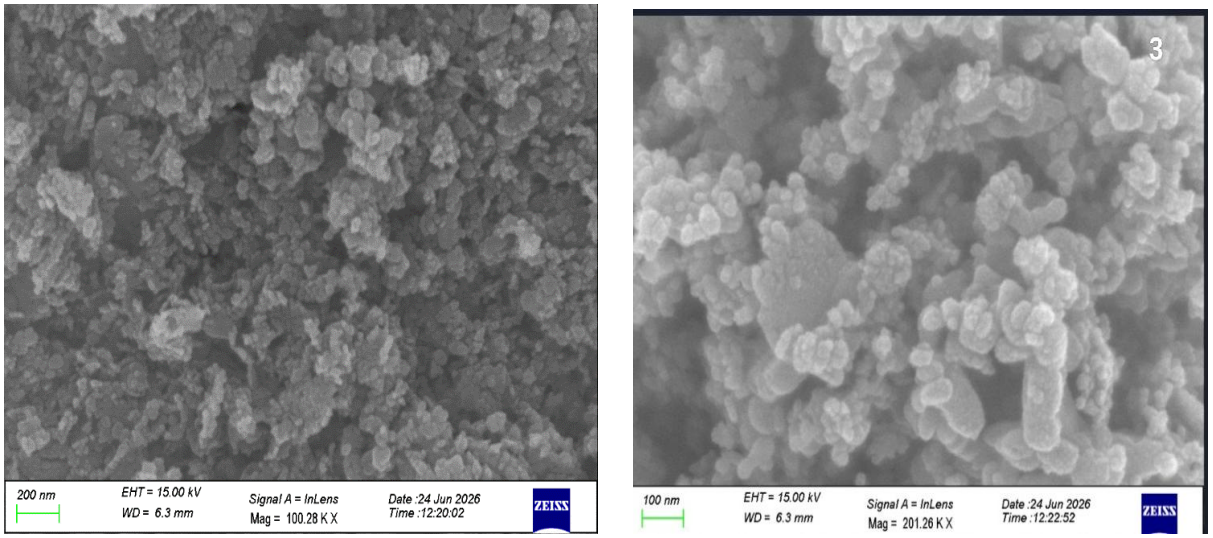


Fig. 4(c): Morphology of sample BR 3 at two different magnifications.

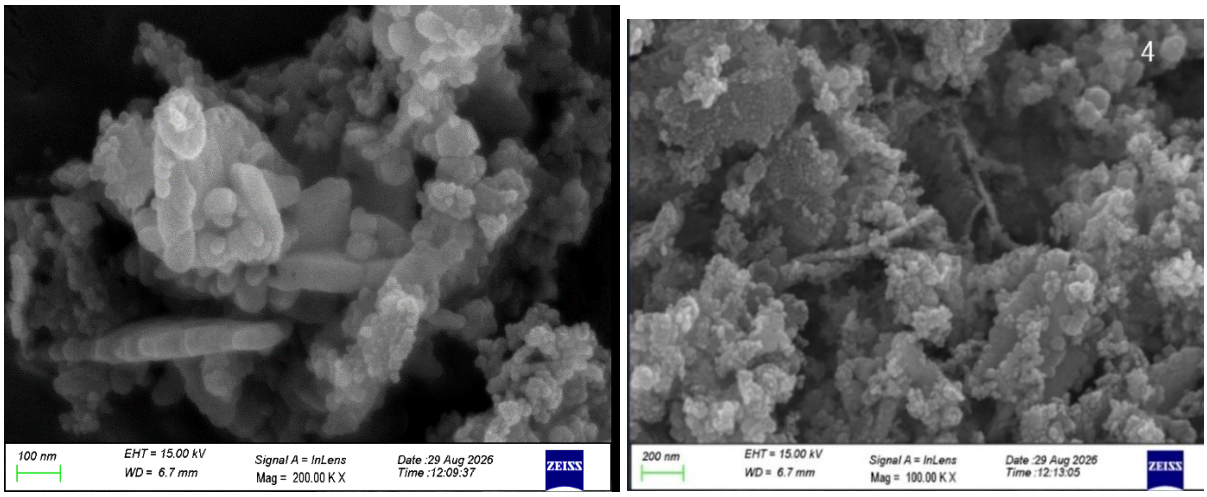


Fig. 4(d): Morphology of sample BR 4 at two different magnifications.

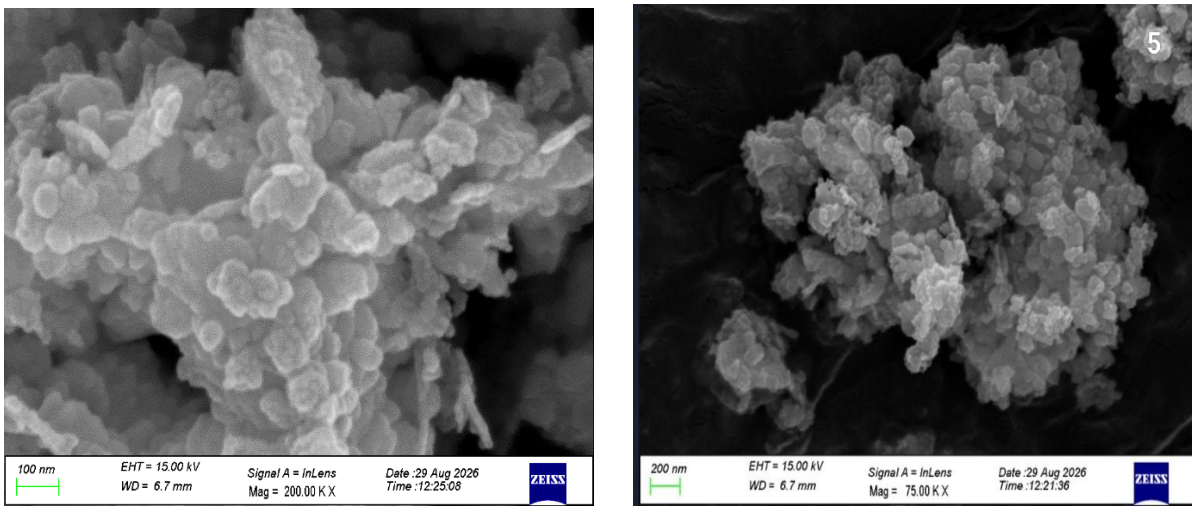
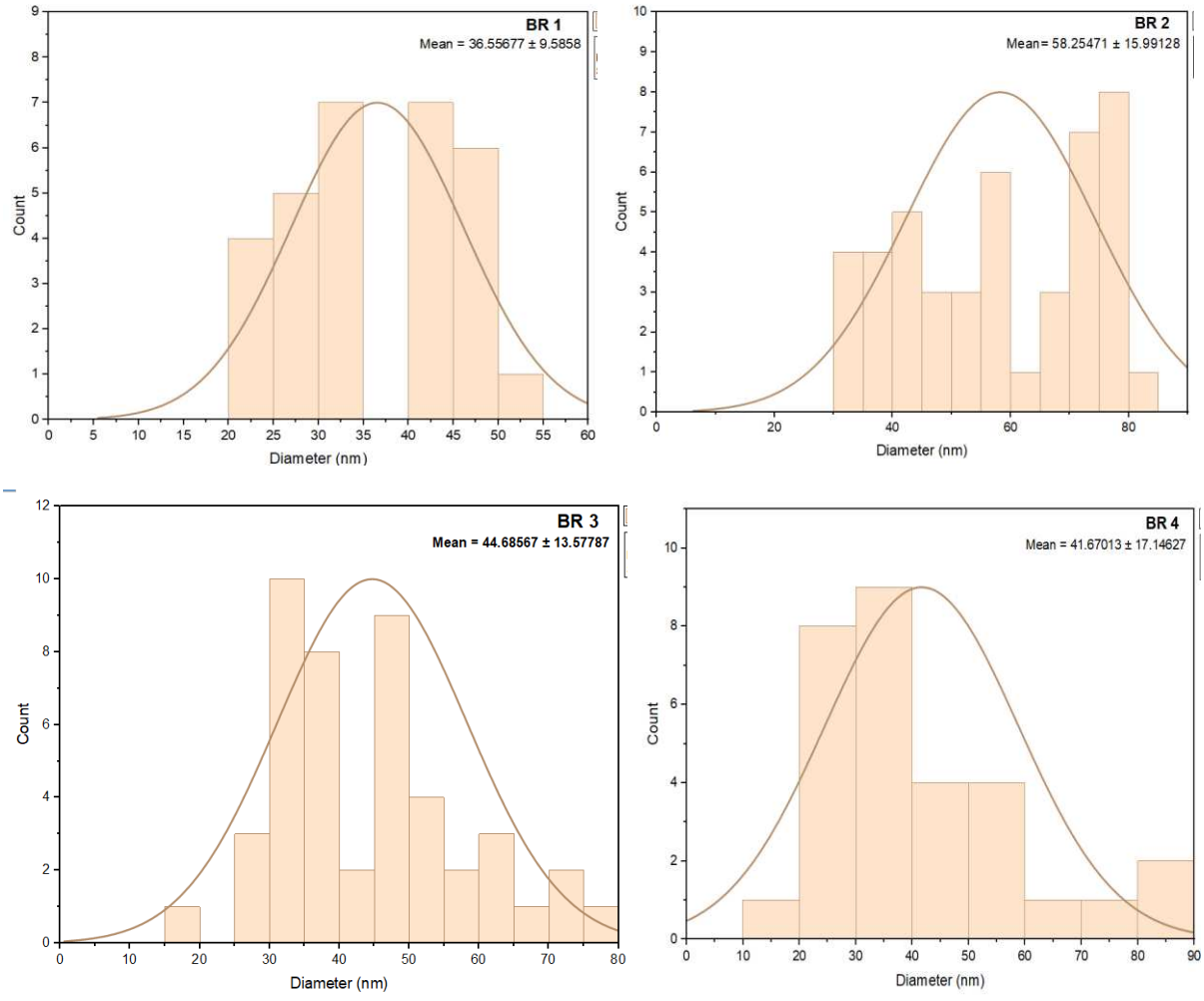


Fig. 4(e): Morphology of sample BR 5 at two different magnifications.

The particle size distributions obtained from the SEM micrographs using ImageJ software displayed in Fig.5. In accordance with its mean of 36.6 ± 9.6 nm and its close, fine clustering in the micrograph, BR 1 provides a reasonably narrow, near-symmetric distribution centered between 30-45 nm (two adjacent bins each containing seven of the 30 particles examined). With a wider, right-skewed distribution and a secondary shoulder near 55-60 nm in addition to its primary peak at 70-75 nm (mean 58.3 ± 16.0 nm), BR 2 is both larger and more dispersed, indicating two overlapping populations of particle sizes rather than a single uniform growth event. With peaks at 30-35 nm and 45-50 nm (mean 44.7 ± 13.6 nm), BR 3 exhibits a similarly bimodal tendency, reflecting the combined sheet-like and spherical morphology seen in its micrograph. BR 4's distribution is left-leaning and comparatively broad (10–90 nm range, mean 41.7 ± 17.1 nm), with most particles falling below 40 nm but a small tail of larger agglomerates extending toward 90 nm, matching the coarser, angular clusters observed. BR 5 has a dominant peak at 50–60 nm (15 of 39 particles measured) with a moderate right-hand tail extending past 100 nm, giving it the largest mean of the series (62.7 ± 19.1 nm) despite most individual particles clustering in a comparatively tight range, reflecting the large, dense agglomerates visible in its micrograph. Overall, the width and skew of each histogram not just the mean tracks the qualitative agglomeration behaviour seen in the corresponding micrographs narrower, more symmetric distributions (BR 1) correspond to finer, less-aggregated particles, while broader or right-skewed distributions with secondary peaks (BR 2, BR 3) correspond to samples with a visible mix of fine and coarser particles.



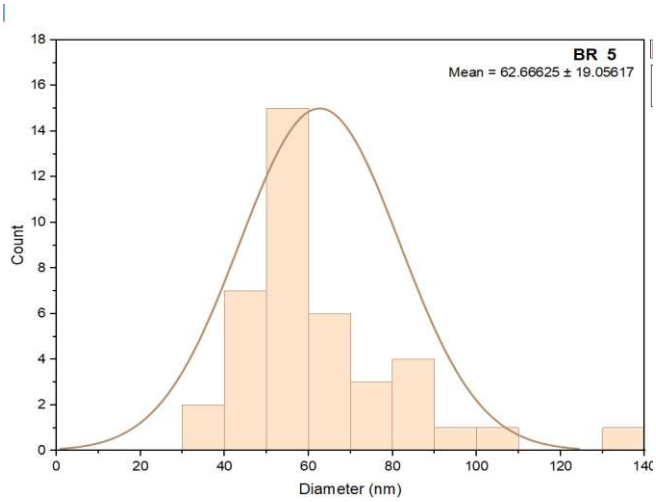


Fig 5: Particle size distribution of synthesized ZnO nanoparticles from SEM Image analysis for BR 1-BR 5.

Synthesis: Relating Physicochemical Properties Across Blends

Taken together, the characterization data confirm the presence of ZnO nanoparticles in all five blend treatments, however, it is clear that the presence of the different blend ratios significantly affected the morphology, size and colloidal behavior of the resulting nanoparticles, with comparatively little impact on the underlying electronic structure (band gap values showed very little variance based on blend ratio).

Seed germination and seedling growth response

All the groups treated with nanoparticles had either a similar or higher germination percentage compared with the distilled water (DW) as control, presented in Table 2 and seedling growth with respect to shoot and root length shown in Fig.6. The germination percentage was 93.34% in the control group, whereas the nanoparticle-treated groups showed germination percentage ranging from 96.67% to 100%. In most of the treated groups, germination was at or near 100%, suggesting seedling growth to be a more sensitive indicator of the functional performance of the formulation.

Shoots and roots exhibited the same growth trends for all the blend ratios. Both parameters increased toward the intermediate blends and reached their maximum in the 50:50 treatment before declining at higher chickpea-husk proportions. The 50:50 formulation also gave the highest vigor index, demonstrating the greatest overall enhancement of early seedling performance.

Table 2. Germination percentage, seedling growth, and vigor index by treatment group

Group	Shoot length (cm)	Root length (cm)	Germination (%)	Vigor index

DW Control	2.65	1.73	93.34	4.09
100% Amla	3.17	1.95	100	5.22
75:25	4.18	2.52	100	6.70
50:50	4.40	2.59	100	6.99
25:75	3.54	2.24	100	5.78
100% Husk	3.34	1.92	96.67	5.09

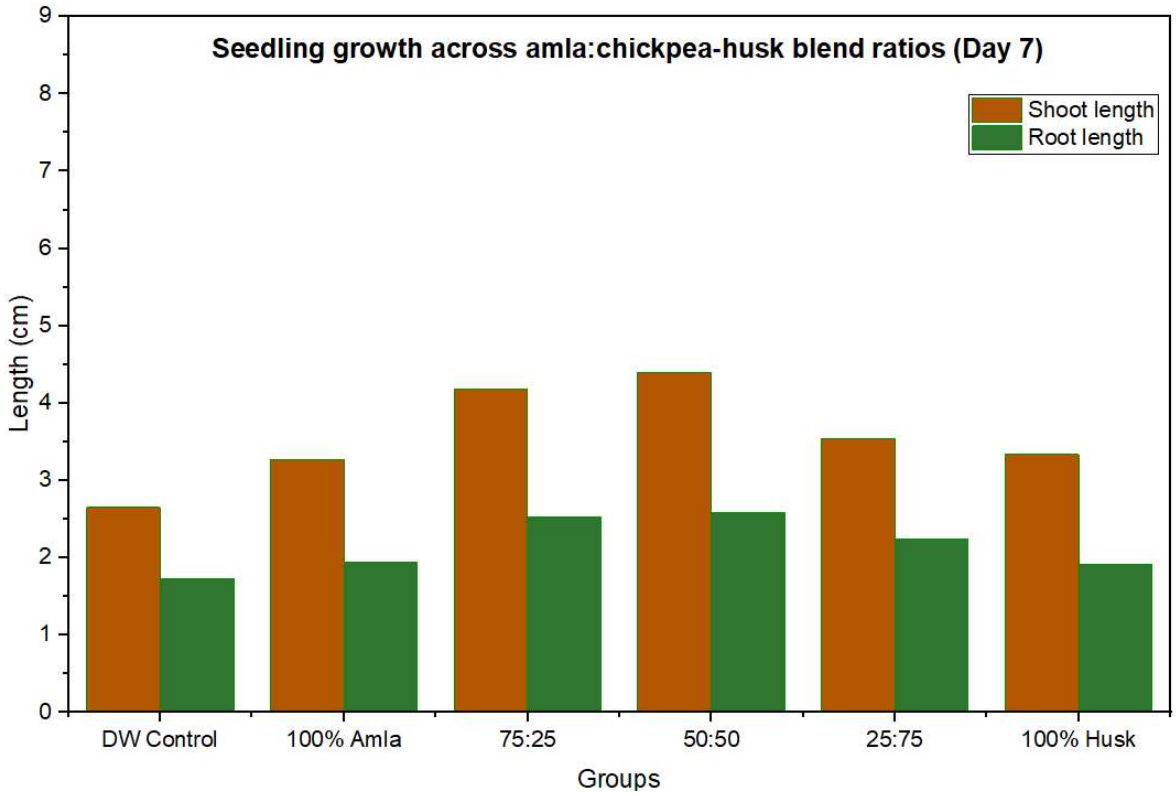


Fig. 6 Effect of amla:chickpea-husk ZnO nanoparticle blend treatments on shoot length and root length.

The growth-promoting effect observed was consistent with previous studies on ZnO nanopriming. ZnO nanoparticles have been reported to enhance germination, water uptake, α-amylase activity, seedling vigor, and photosynthetic performance in wheat plants [55]. Other studies have also demonstrated improvements in early seedling growth depending on the concentration applied, with beneficial growth effects observed within the optimal treatment range [56,57].

The present experiment differs from conventional nanoparticles dose-response studies because nanoparticles exposure was fixed across the treatments. Therefore, the differences in seedling performance reflect the properties of the nanoparticles synthesized from different extract compositions rather than differences in the quantity of nanoparticles exposed to the seeds.

Relationship between extract or nanoparticle properties and seedling growth

All measurements for the blend compositions were averaged and Pearson's correlations and Pairwise scatterplot matrix was calculated for each sample summarized in Table 3 and Fig.7 respectively. The analysis showed a strong positive relationship between DPPH inhibition and shoot length and root length. In contrast, carbohydrate, protein, and particle diameter did not show meaningful correlations with shoot or root length.

An additional inverse correlation was observed between protein content and nanoparticle diameter (r = -0.879, p =0.0495). Thus, blends with higher measured protein content tended to produce smaller ZnO nanoparticles. This relationship was not reflected in the protein-growth correlations, which remained weak for both shoot and root length. Protein content therefore appears to be more closely associated with nanoparticle formation and size regulation than with seedling growth directly. Plant-derived proteins can adsorb onto developing nanoparticle surfaces and act as biogenic capping or stabilizing molecules, thereby limiting aggregation and influencing particle growth [8,13].

Table 3. Pearson correlation matrix (r), degrees of freedom, exact p-values between extract/nanoparticle properties (DPPH, carbohydrate, protein, particle size) and growth metrics (shoot length, root length) across the five blend-level means (n = 5). * p < .05.

Correlation Matrix							
		DPPH	Carb	Proteins	Size	Shoot	Root
DPPH	Pearson's r	—					
	df	—					
	p-value	—					
Carb	Pearson's r	0.491	—				
	df	3	—				
	p-value	.401	—				
Proteins	Pearson's r	-0.162	0.163	—			
	df	3	3	—			
	p-value	.794	.793	—			
Size	Pearson's r	-0.101	-0.584	-0.879*	—		
	df	3	3	3	—		
	p-value	.872	.301	.050	—		
Shoot	Pearson's r	0.892*	0.068	-0.241	0.178	—	
	df	3	3	3	3	—	
	p-value	.042	.913	.696	.775	—	
Root	Pearson's r	0.889*	0.179	-0.077	0.023	0.970**	—
	df	3	3	3	3	3	—
	p-value	.044	.774	.902	.971	.006	—

Note. * p < .05, ** p < .01, *** p < .001

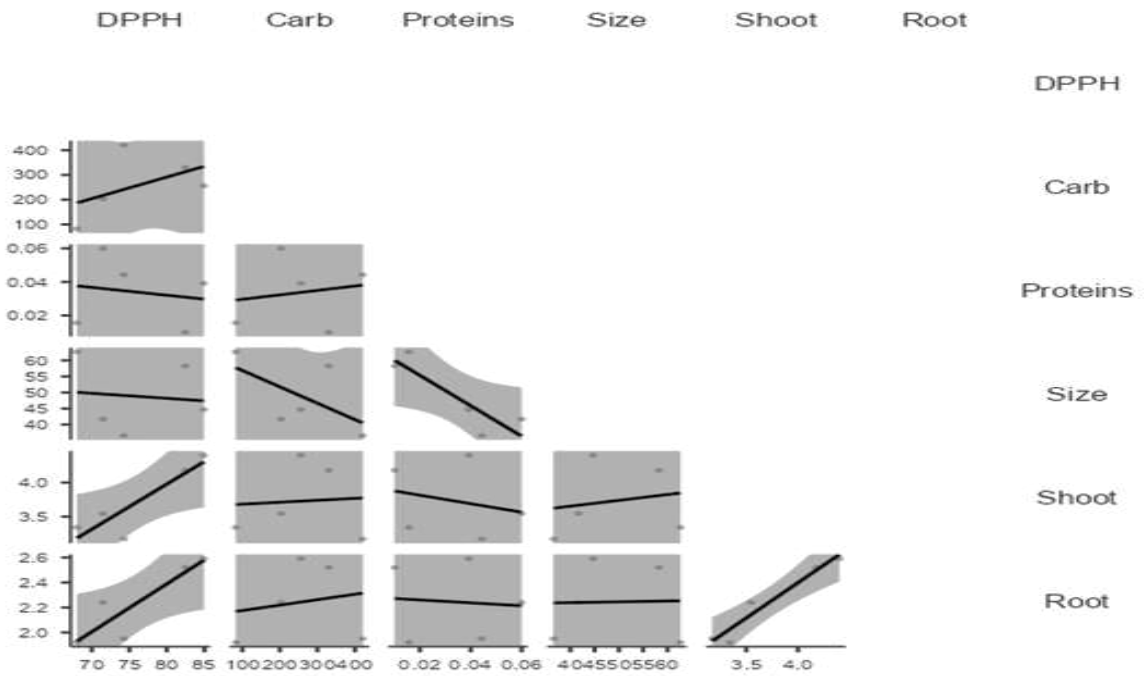


Fig.7 Pairwise scatterplot matrix illustrating relationships among extract/nanoparticle properties and growth metrics across the five blend-level means (n = 5).

Among the measured extract and nanoparticle properties, DPPH exhibited the highest correlation with growth-promoting performance i.e. shoot and root development; while no relationship was observed between particle diameter and either of the two biological responses. The inverse relationship between protein content and particle diameter provides a second level of interpretation for the blend-dependent synthesis results. Protein content did not predict shoot or root growth, but it was strongly associated with nanoparticle size, indicating that protein-rich extract compositions influenced the physical formation of the nanoparticles. This finding separates the factors controlling nanoparticle production from those most closely associated with plant response. In the present system, protein content was linked primarily to particle-size regulation, whereas DPPH activity showed the strongest relationship with seedling growth. The data therefore support a two-stage interpretation in which extract proteins influence nanoparticle formation and stabilization, while the broader antioxidant and surface-chemical profile of the extract determines biological performance.

Optimum response

In this study, antioxidant capacity was found to be the strongest measured compositional factor affecting the performance of ZnO nanoparticles, whereas particle diameter did not follow the same trend as the biological responses. DPPH-growth correlation can be explained by the chemical processes that occur during nanoparticle synthesis using plants. The phytochemicals responsible for antioxidant activity may also play a role in precursor reduction, nucleation, and functionalization of the nanoparticle surfaces. These interactions can contribute to changes in the surface chemistry of nanoparticles, which may influence their dispersion, interactions with plant tissues, dissolution, as well as zinc availability [8,13]. ZnO nanoparticles can affect several processes associated with early plant growth. ZnO nanopriming enhances uptake of

water and α-amylase activity during germination, suggesting that these effects may facilitate the mobilization of stored seed reserves and support early embryo growth [55].

Although DPPH inhibition showed strong positive correlations with both shoot and root length, these relationships should be interpreted within the limits of the formulation design. The correlation analysis was based on five distinct amla-chickpea husk blend compositions, and correlations calculated from a small number of formulation points can be sensitive to the position of individual observations and may not provide stable estimates of the broader population relationship [58,59]. This limitation does not reflect a lack of experimental replication as each formulation was tested with replicate measurements. Rather, it reflects the restricted number of composition levels used to describe the formulation space. The present findings, therefore, indicate strong evidence of the association between antioxidant capacity and ZnO nanoparticle induced seedling growth. Future studies should expand the plant extract gradient by including additional blend ratios while retaining independent synthesis and biological replicates. Including more systematically varied blend ratios would provide a clearer understanding of how changes in extract composition affect nanoparticle properties and their biological activity, while also enabling response surface methodology to identify blend ratios associated with desirable nanoparticle properties and biological performance.

The 50:50 formulation's superior performance did not follow a typical concentration-dependent pattern but was associated with the optimum blend composition. The intermediate blend gave the best response, whereas both extremes of the blend range were less effective. The 100% amla and 100% chickpea husk treatments were not as biologically beneficial as the combined extracts. This indicates that the interaction between the two extract chemistries. This result is consistent with earlier findings showing that changes in green synthesis parameters can influence nanoparticle properties in a nonlinear manner. Different synthesis ratios can affect properties such as particle size and stability, although the nature and strength of these effects may vary depending on the preparation conditions and the properties being evaluated [60]. Particle diameter itself showed no relationship with seedling growth. Although the protein–diameter correlation was statistically significant, particle diameter itself was unrelated to shoot or root length, indicating that the protein-associated reduction in particle size did not translate directly into enhanced seedling growth. This finding does not indicate that particle size is irrelevant in all plant-nanoparticle synthesis. Particle size can influence the dissolution, uptake, transport, and interactions with plant tissues depending on the surrounding medium and surface chemistry [29].

Present result establishes that particle diameter was not the dominant property separating the five formulations tested here. These observations are consistent with the findings of [36], who observed similar effects on onion germination and seedling growth following the application of submicron ZnO and ZnO nanoparticles. Their results suggest that the particle size may not have had as much influence as zinc-ion availability in this system. Therefore, these biological differences may be more closely related to surface chemistry, colloidal stability, dissolution behaviour, and zinc availability than to the particle diameter alone.

Conclusion

The extract composition of the amla:chickpea-husk blends influenced DPPH antioxidant activity, which emerged as the strongest parameter associated with growth-promoting performance of the synthesized nanoparticles among the biochemical and physicochemical properties tested. The connections between particle size, protein and carbohydrate contents

with the growth response were weak and non-significant. The intermediate 50:50 blend had the highest DPPH activity, and shoot growth and root growth showed a similar pattern. Neither the growth parameters nor the DPPH activity showed a dominant correlation with the particle size. This suggests that the functional performance of the nanoparticles in the current system is more closely associated with the biochemical composition of the extracts than on their physical size. Overall, the findings support extract-composition tuning as a promising and previously underexplored variable in green-synthesis nano agriculture.

Acknowledgement: The author extends their appreciation to the Principal of Ramjas College, University of Delhi, and the Ministry of Fisheries, Animal Husbandry and Dairying of India.

Author Contributions

A.G.- Conceptualization , wrote the manuscript draft, formal analysis, review and editing, data finalization

S.A.-wrote the manuscript draft, Review and editing, formal analysis, Conceptualization and data finalization.

N.N- Validation, wrote the manuscript draft Conceptualization, and formal analysis

S.- Draw Graph and image, wrote the final manuscript draft and Review and editing

S.R.- Draw Graph and image, wrote the final manuscript draft and Review and editing

A.M.- Methodology, review & editing, Validation and formal analysis

P.S., - Methodology, review & editing, Validation

S.V.-Conceptualization, review and editing, validation, visualization, supervision and formal analysis.

Funding Agency

This study is part of the Production of Cow-Bioplastic from Cow dung and its applications in different areas, Sponsored by the Ministry of Fisheries, Animal Husbandry and Dairying, Delhi, India, R-30012/1/2022-DADF-Dept-Part (2) (E-24308).

Data availability statement:

The author confirms that the data supporting the findings of this study are available in the article

Conflict of interest:

The authors declare no conflicts of interest regarding this study.

Declaration of competing interest

For this study, the authors disclose no conflicts of interest.

Reference

1. Arora, S., Murmu, G., Mukherjee, K., Saha, S., & Maity, D. (2022). A comprehensive overview of nanotechnology in sustainable agriculture. *Journal of Biotechnology*, *355*, 21–41. https://doi.org/10.1016/j.jbiotec.2022.06.007

2. Usman, M., Farooq, M., Wakeel, A., Nawaz, A., Cheema, S. A., Rehman, H. ur, Ashraf, I., & Sanaullah, M. (2020). Nanotechnology in agriculture: Current status, challenges and future opportunities. *Science of The Total Environment*, *721*, 137778. https://doi.org/10.1016/j.scitotenv.2020.137778

3. Okey-Onyesolu, C. F., Hassanisaadi, M., Bilal, M., Barani, M., Rahdar, A., Iqbal, J., & Kyzas, G. Z. (2021). Nanomaterials as Nanofertilizers and Nanopesticides: An Overview. *ChemistrySelect*, *6*(33), 8645–8663. https://doi.org/10.1002/slct.202102379

4. Tang, Y., Zhao, W., Zhu, G., Tan, Z., Huang, L., Zhang, P., Gao, L., & Rui, Y. (2023). Nano-Pesticides and Fertilizers: Solutions for Global Food Security. *Nanomaterials*, *14*(1), 90. https://doi.org/10.3390/nano14010090

5. Ayub, A., Wani, A. K., Malik, S. M., Ayub, M., Singh, R., Chopra, C., & Malik, T. (2025). Green nanoscience for healthcare: Advancing biomedical innovation through eco-synthesized nanoparticle. *Biotechnology Reports*, *47*, e00913. https://doi.org/10.1016/j.btre.2025.e00913

6. Jain, A. S., Pawar, P. S., Sarkar, A., Junnuthula, V., & Dyawanapelly, S. (2021). Bionanofactories for Green Synthesis of Silver Nanoparticles: Toward Antimicrobial Applications. *International Journal of Molecular Sciences*, *22*(21), 11993. https://doi.org/10.3390/ijms222111993

7. Soni, V., Raizada, P., Singh, P., Cuong, H. N., S, R., Saini, A., Saini, R. V., Le, Q. Van, Nadda, A. K., Le, T.-T., & Nguyen, V.-H. (2021). Sustainable and green trends in using plant extracts for the synthesis of biogenic metal nanoparticles toward environmental and pharmaceutical advances: A review. *Environmental Research*, *202*, 111622. https://doi.org/10.1016/j.envres.2021.111622

8. Khan, F., Shariq, M., Asif, M., Siddiqui, M. A., Malan, P., & Ahmad, F. (2022). Green Nanotechnology: Plant-Mediated Nanoparticle Synthesis and Application. *Nanomaterials*, *12*(4), 673. https://doi.org/10.3390/nano12040673

9. Shafey, A. M. El. (2020). Green synthesis of metal and metal oxide nanoparticles from plant leaf extracts and their applications: A review. *Green Processing and Synthesis*, *9*(1), 304–339. https://doi.org/10.1515/gps-2020-0031

10. Singh, H., Desimone, M. F., Pandya, S., Jasani, S., George, N., Adnan, M., Aldarhami, A., Bazaid, A. S., & Alderhami, S. A. (2023). Revisiting the Green Synthesis of Nanoparticles: Uncovering Influences of Plant Extracts as Reducing Agents for Enhanced Synthesis Efficiency and Its Biomedical Applications. *International Journal of Nanomedicine*, *Volume 18*, 4727–4750. https://doi.org/10.2147/IJN.S419369

11. Haiouani, K., Hegazy, S., Alsaeedi, H., Bechelany, M., & Barhoum, A. (2024). Green Synthesis of Hexagonal-like ZnO Nanoparticles Modified with Phytochemicals of Clove (Syzygium aromaticum) and Thymus capitatus Extracts: Enhanced Antibacterial, Antifungal, and Antioxidant Activities. *Materials*, *17*(17), 4340. https://doi.org/10.3390/ma17174340

12. Al-Hakkani, M. F. (2020). Biogenic copper nanoparticles and their applications: A review. *SN Applied Sciences*, *2*(3), 505. https://doi.org/10.1007/s42452-020-2279-1

13. Sidhu, A. K., Verma, N., & Kaushal, P. (2022). Role of Biogenic Capping Agents in the Synthesis of Metallic Nanoparticles and Evaluation of Their Therapeutic Potential. *Frontiers in Nanotechnology*, *3*. https://doi.org/10.3389/fnano.2021.801620

14. Villagrán, Z., Anaya-Esparza, L. M., Velázquez-Carriles, C. A., Silva-Jara, J. M., Ruvalcaba-Gómez, J. M., Aurora-Vigo, E. F., Rodríguez-Lafitte, E., Rodríguez-Barajas, N., Balderas-León, I., & Martínez-Esquivias, F. (2024). Plant-Based Extracts as Reducing, Capping, and Stabilizing Agents for the Green Synthesis of Inorganic Nanoparticles. *Resources*, *13*(6), 70. https://doi.org/10.3390/resources13060070

15. Huang, J. (2025). Toward Safer Nanotechnology: Eco-friendly Strategies for Nanoparticle Fabrication. *Advances in Engineering Technology Research*, *15*(1), 1822. https://doi.org/10.56028/aetr.15.1.1822.2025

16. Kar, A. K., Shraogi, N., Saji, J., Verma, R., Singh, D., Singh, A., Ghosh, D., & Patnaik, S. (2025). Comparative study on green versus chemical synthesis for metallic NPs with respect to physicochemical characterization and toxicity. *Next Materials*, *9*, 101184. https://doi.org/10.1016/j.nxmate.2025.101184

17. Antunes Filho, S., dos Santos, M. S., dos Santos, O. A. L., Backx, B. P., Soran, M.-L., Opriş, O., Lung, I., Stegarescu, A., & Bououdina, M. (2023). Biosynthesis of Nanoparticles Using Plant Extracts and Essential Oils. *Molecules*, *28*(7), 3060. https://doi.org/10.3390/molecules28073060

18. Janah, I. M., Roto, R., & Siswanta, D. (2022). Effect of Ascorbic Acid Concentration on the Stability of Tartrate-Capped Silver Nanoparticles. *Indonesian Journal of Chemistry*, *22*(1), 857. https://doi.org/10.22146/ijc.73196

19. Behtash, F., Amini, T., Mousavi, S. B., Seyed Hajizadeh, H., & Kaya, O. (2024). Efficiency of zinc in alleviating cadmium toxicity in hydroponically grown lettuce (Lactuca sativa L. cv. Ferdos). *BMC Plant Biology*, *24*(1), 648. https://doi.org/10.1186/s12870-024-05325-9

20. Hosamani, V., Yalagi, M., Sasvihalli, P., Hosamani, V., Nair, K. S., Harlapur, V., Hegde, C., & Mishra, R. (2020). Importance of micronutrients (Zinc) in crop production: A review. *International Journal of Chemical Studies*, *8*(1), 1060–1064. https://doi.org/10.22271/chemi.2020.v8.i1n.8393

21. Pasternak, T. P., & Steinmacher, D. (2024). Plant Growth Regulation in Cell and Tissue Culture In Vitro. *Plants*, *13*(2), 327. https://doi.org/10.3390/plants13020327

22. Ashokkumar, K., Sasikala, P., Murugan, M., Muthukrishnan, S., & Dhanya, M. K. (2026). Insights into green synthesized zinc oxide nanoparticles for abiotic stress tolerance, crop growth and development. *Discover Plants*, *3*(1), 39. https://doi.org/10.1007/s44372-026-00504-4

23. Sarkhosh, S., Kahrizi, D., Darvishi, E., Tourang, M., Haghighi-Mood, S., Vahedi, P., & Ercisli, S. (2022). Effect of Zinc Oxide Nanoparticles (ZnO-NPs) on Seed Germination Characteristics in Two Brassicaceae Family Species: *Camelina sativa* and *Brassica napus L. Journal of Nanomaterials*, *2022*(1). https://doi.org/10.1155/2022/1892759

24. Naseer, I., Javed, S., Shah, A. A., Tariq, A., & Ahmad, A. (2024). Influence of phyto-mediated zinc oxide nanoparticles on growth of (Zea mays L.). *Pakistan Journal of Botany*, *56*(3). https://doi.org/10.30848/PJB2024-3(7)

25. Ukidave, V. V., & Ingale, L. T. (2022). Green Synthesis of Zinc Oxide Nanoparticles from Coriandrum sativum and Their Use as Fertilizer on Bengal Gram, Turkish Gram, and Green Gram Plant Growth. *International Journal of Agronomy*, *2022*, 1–14. https://doi.org/10.1155/2022/8310038

26. Djanaguiraman, M., Anbazhagan, V., Dhankher, O. P., & Prasad, P. V. V. (2024). Uptake, Translocation, Toxicity, and Impact of Nanoparticles on Plant Physiological Processes. *Plants*, *13*(22), 3137. https://doi.org/10.3390/plants13223137

27. Umar, W., Czinkota, I., Gulyás, M., Ayub, M. A., Sebők, A., Nadeem, M. Y., & Zulfiqar, M. A. (2023). Effect of Soil Texture, Nanoparticle Size, and Incubation Period on the Dissolution of ZnO Nanoparticles. *Pollutants*, *3*(2), 220–231. https://doi.org/10.3390/pollutants3020016

28. Yan, N., Wang, Y., Wong, T. Y., Wu, Z., Wang, X., Xie, M., Kutumova, E., Parodi, A., Kolpakov, F., Wang, W.-X., & Shi, J. (2025). Differential Mapping of Intracellular Metallic Nanoparticles and Ions and Dynamic Modeling Prediction. *ACS Nano*, *19*(23), 21644–21659. https://doi.org/10.1021/acsnano.5c04379

29. da Cruz, T. N. M., Savassa, S. M., Montanha, G. S., Ishida, J. K., de Almeida, E., Tsai, S. M., Lavres Junior, J., & Pereira de Carvalho, H. W. (2019). A new glance on root-to-shoot in vivo zinc transport and time-dependent physiological effects of ZnSO4 and ZnO nanoparticles on plants. *Scientific Reports*, *9*(1), 10416. https://doi.org/10.1038/s41598-019-46796-3

30. Savassa, S. M., Duran, N. M., Rodrigues, E. S., de Almeida, E., van Gestel, C. A. M., Bompadre, T. F. V., & P. de Carvalho, H. W. (2018). Effects of ZnO Nanoparticles on *Phaseolus vulgaris* Germination and Seedling Development Determined by X-ray Spectroscopy. *ACS Applied Nano Materials*, *1*(11), 6414–6426. https://doi.org/10.1021/acsanm.8b01619

31. Paranimuthu, S., Pandey, R., Yadav, A., Gowda, V. T., Krishnan, P., Sharma, D. K., Shankar, V., Eere, V. M., Jagadam, S. R., Ranjan, R., Bana, R. S., & Kumar, A. (2026). Size dependent efficacy of zinc oxide nanoparticles in zinc biofortification of basmati rice. *Scientific Reports*, *16*(1), 8886. https://doi.org/10.1038/s41598-025-30827-3

32. Balusamy, S. R., Joshi, A. S., Perumalsamy, H., Mijakovic, I., & Singh, P. (2023). Advancing sustainable agriculture: a critical review of smart and eco-friendly nanomaterial applications. *Journal of Nanobiotechnology*, *21*(1), 372. https://doi.org/10.1186/s12951-023-02135-3

33. Barbinta-Patrascu, M.-E., Bita, B., & Negut, I. (2024). From Nature to Technology: Exploring the Potential of Plant-Based Materials and Modified Plants in Biomimetics, Bionics, and Green Innovations. *Biomimetics*, *9*(7), 390. https://doi.org/10.3390/biomimetics9070390

34. Kumarasamy, R. V., Natarajan, P. M., Mathivanan, I., Balasubramaniam, M., SN, S., Prabhu, D., Raju, K., Mironescu, M., & Mironescu, I. D. (2026). Sustainable biogenic synthesis of silver nanoparticles for oral cancer: a comprehensive review. *Frontiers in Nanotechnology*, *7*. https://doi.org/10.3389/fnano.2025.1648900

35. Trzcińska-Wencel, J., Mucha, N., Rai, M., Tyburski, J., & Golińska, P. (2025). Pre-sowing grain treatment with bio-AgNPs stimulates plant growth and affects redox homeostasis in maize. *Frontiers in Plant Science*, *16*. https://doi.org/10.3389/fpls.2025.1494741

36. Tymoszuk, A., & Wojnarowicz, J. (2020). Zinc Oxide and Zinc Oxide Nanoparticles Impact on In Vitro Germination and Seedling Growth in Allium cepa L. *Materials*, *13*(12), 2784. https://doi.org/10.3390/ma13122784

37. Fatima, E., Arooj, I., Javeed, M., & Yin, J. (2024). Green synthesis, characterization and applications of Phyllanthus emblica fruit extract mediated chromium oxide nanoparticles. *Discover Nano*, *19*(1), 68. https://doi.org/10.1186/s11671-024-04006-8

38. Niño-Medina, G., Muy-Rangel, D., de la Garza, A. L., Rubio-Carrasco, W., Pérez-Meza, B., Araujo-Chapa, A. P., Gutiérrez-Álvarez, K. A., & Urías-Orona, V. (2019). Dietary Fiber from Chickpea (Cicer arietinum) and Soybean (Glycine max) Husk Byproducts as Baking Additives: Functional and Nutritional Properties. *Molecules*, *24*(5), 991. https://doi.org/10.3390/molecules24050991

39. Singdam, P., Kamnate, A., Somsap, O.-A., & Tohkayomatee, R. (2025). Phytochemical Screening, Antioxidant Potential, and α-Glucosidase Inhibition of Causonis trifolia Leaf Extracts: A Solvent-Based Comparative Study. *Pharmacognosy Journal*, *17*(2), 164–170. https://doi.org/10.5530/pj.2025.17.20

40. Tamboli, F. A., More, H. N., Bhandugare, S. S., Patil, A. S., Jadhav, N. R., & Killedar, S. G. (2020). Estimation of Total Carbohydrate content by Phenol Sulphuric acid Method from Eichhornia crassipes (Mart.) Solms. *Asian Journal Of Research in Chemistry*, *13*(5), 357–359. https://doi.org/10.5958/0974-4150.2020.00067.X

41. Ngo, A. N. (2014). Optimal Concentration of 2,2,2-Trichloroacetic Acid for Protein Precipitation Based on Response Surface Methodology. *Journal of Analytical & Bioanalytical Techniques*, *5*(4). https://doi.org/10.4172/2155-9872.1000198

42. Charles, D. A., Katturajan, R., Kumar, G., Velu, S., Nisar, N. T., & Prince, S. E. (2025). Green Synthesis of ZnO Nanoparticles from Caesalpinia bonducella Seed and Application in Nano-priming-Assisted Vigna mungo Seed Germination. *International Journal of Scientific Research and Modern Technology (IJSRMT)*, *4*(1), 37–48. https://doi.org/10.5281/zenodo.14745500

43. Kurdekar, A. K., Desai, B. K., Koppalakar, B. G., Sannagoudar, M. S., Rathod, P. S., Hiregoudar, S., Rajesh, N. L., Almutairi, K. F., Elansary, H. O., & Nazim, M. (2025). Comparative evaluation of green synthesized and commercial iron and zinc nanoparticles on germination, growth and productivity of pigeonpea. *Scientific Reports*, *15*(1), 25956. https://doi.org/10.1038/s41598-025-96441-5

44. Katiyar, A., Kumar, N., Shukla, R. K., & Srivastava, A. (2020). Substrate free ultrasonic-assisted hydrothermal growth of ZnO nanoflowers at low temperature. *SN Applied Sciences*, *2*(8), 1386. https://doi.org/10.1007/s42452-020-3186-1

45. Maher, S., Nisar, S., Aslam, S. M., Saleem, F., Behlil, F., Imran, M., Assiri, M. A., Nouroz, A., Naheed, N., Khan, Z. A., & Aslam, P. (2023). Synthesis and

Characterization of ZnO Nanoparticles Derived from Biomass (*Sisymbrium Irio*) and Assessment of Potential Anticancer Activity. *ACS Omega*, *8*(18), 15920–15931. https://doi.org/10.1021/acsomega.2c07621

46. Al-Shehaby, N., Elshoky, H. A., Zidan, M., Salaheldin, T. A., Gaber, M. H., Ali, M. A., & El-Sayed, N. M. (2025). In vitro localization of modified zinc oxide nanoparticles showing selective anticancer effects against colorectal carcinoma using biophysical techniques. *Scientific Reports*, *15*(1), 16811. https://doi.org/10.1038/s41598-025-00434-3

47. Bin Fazal, D., & Ahmad, I. (2024). A critical analysis of extracts of okra seeds and amla offering green chemistry for synthesis of zinc oxide nanoparticles and their promising role in reducing crude oil viscosity. *Materials Today Communications*, *38*, 108172. https://doi.org/10.1016/j.mtcomm.2024.108172

48. Hamed, R., Obeid, R. Z., & Abu-Huwaij, R. (2023). Plant mediated-green synthesis of zinc oxide nanoparticles: An insight into biomedical applications. *Nanotechnology Reviews*, *12*(1). https://doi.org/10.1515/ntrev-2023-0112

49. Maher, S., Zamina, B., Riaz, M., Riaz, S., Khalid, N., Imran, M., Fahmid, S., Ishtiaq, H., & Parveen, S. (2023). Green Synthesis of *Withania coagulans* Extract-Mediated Zinc Oxide Nanoparticles as Photocatalysts and Biological Agents. *ACS Omega*, *8*(49), 46715–46727. https://doi.org/10.1021/acsomega.3c05947

50. Al-Zahrani, S. A., Umar, K., Tweib, S. A., Rashd, J. A. M., Afridi, S. K., Bhawani, S. A., Otaibi, A. Al, Masood, N., Mansour, D., Khan, A., & Ayyar, M. (2023). Biomass Mediated Synthesis of ZnO and ZnO/GO for the Decolorization of Methylene Blue under Visible Light Source. *Catalysts*, *13*(2), 409. https://doi.org/10.3390/catal13020409

51. Vera, J., Herrera, W., Hermosilla, E., Díaz, M., Parada, J., Seabra, A. B., Tortella, G., Pesenti, H., Ciudad, G., & Rubilar, O. (2023). Antioxidant Activity as an Indicator of the Efficiency of Plant Extract-Mediated Synthesis of Zinc Oxide Nanoparticles. *Antioxidants*, *12*(4), 784. https://doi.org/10.3390/antiox12040784

52. Sharma, P., & Sharma, N. (2023). Lignin Derived from Forestry Biomass as Capping Reagent in the Biosynthesis and Characterization of Zinc Oxide Nanoparticles and Their In Vitro Efficacy as a Strong Antifungal Biocontrolling Agent for Commercial Crops. *BioNanoScience*, *13*(1), 36–48. https://doi.org/10.1007/s12668-022-01052-3

53. Barani, D., Tedjani, M. L., Younes, Z., Meneceur, S., Laouini, S. E., & Hammami, H. (2023). Biomass-mediated synthesis of ZnO and Mg@ZnO nanoparticles for enhancing the degradation of m-toluidine and p-toluidine. *Biomass Conversion and Biorefinery*, *13*(8), 7311–7318. https://doi.org/10.1007/s13399-022-03411-2

54. Okpara, E. C., Fayemi, O. E., Sherif, E.-S. M., Junaedi, H., & Ebenso, E. E. (2020). Green Wastes Mediated Zinc Oxide Nanoparticles: Synthesis, Characterization and Electrochemical Studies. *Materials*, *13*(19), 4241. https://doi.org/10.3390/ma13194241

55. Rai-Kalal, P., & Jajoo, A. (2021). Priming with zinc oxide nanoparticles improve germination and photosynthetic performance in wheat. *Plant Physiology and Biochemistry*, *160*, 341–351. https://doi.org/10.1016/j.plaphy.2021.01.032

56. Donia, D. T., & Carbone, M. (2023). Seed Priming with Zinc Oxide Nanoparticles to Enhance Crop Tolerance to Environmental Stresses. *International Journal of Molecular Sciences*, *24*(24), 17612. https://doi.org/10.3390/ijms242417612

57. Esper Neto, M., Britt, D. W., Lara, L. M., Cartwright, A., dos Santos, R. F., Inoue, T. T., & Batista, M. A. (2020). Initial Development of Corn Seedlings after Seed Priming with Nanoscale Synthetic Zinc Oxide. *Agronomy*, *10*(2), 307. https://doi.org/10.3390/agronomy10020307

58. Bujang, M. A. (2024). An elaboration on sample size determination for correlations based on effect sizes and confidence interval width: a guide for researchers. *Restorative Dentistry & Endodontics*, *49*(2). https://doi.org/10.5395/rde.2024.49.e21

59. Knudson, D. (2025). Confirming Increased Statistical Errors in Testing Correlations from Small Sample Sizes. *Measurement in Physical Education and Exercise Science*, *29*(2), 191–197. https://doi.org/10.1080/1091367X.2024.2439295

60. Sentkowska, A., Folcik, J., Szmytke, J., & Grudniak, A. (2025). Is There Any Correlation Between Green Synthesis Parameters and the Properties of Obtained Selenium Nanoparticles? *Molecules*, *30*(13), 2865. https://doi.org/10.3390/molecules30132865